

Estimate of High Energy Punch-Through in Shielding Wall Cracks

A. J. Stevens

April 1996

Collider Accelerator Department
Brookhaven National Laboratory

U.S. Department of Energy

USDOE Office of Science (SC)

Notice: This technical note has been authored by employees of Brookhaven Science Associates, LLC under Contract No. DE-AC02-76CH00016 with the U.S. Department of Energy. The publisher by accepting the technical note for publication acknowledges that the United States Government retains a non-exclusive, paid-up, irrevocable, world-wide license to publish or reproduce the published form of this technical note, or allow others to do so, for United States Government purposes.

DISCLAIMER

This report was prepared as an account of work sponsored by an agency of the United States Government. Neither the United States Government nor any agency thereof, nor any of their employees, nor any of their contractors, subcontractors, or their employees, makes any warranty, express or implied, or assumes any legal liability or responsibility for the accuracy, completeness, or any third party's use or the results of such use of any information, apparatus, product, or process disclosed, or represents that its use would not infringe privately owned rights. Reference herein to any specific commercial product, process, or service by trade name, trademark, manufacturer, or otherwise, does not necessarily constitute or imply its endorsement, recommendation, or favoring by the United States Government or any agency thereof or its contractors or subcontractors. The views and opinions of authors expressed herein do not necessarily state or reflect those of the United States Government or any agency thereof.

AD/RHIC/RD-97

RHIC PROJECT
Brookhaven National Laboratory

Energy Deposition Downstream of the Internal Dump

A. J. Stevens

December 1995

Energy Deposition Downstream of the Internal Dump

I. Introduction

This note presents the results of recent CASIM calculations of energy deposition in the coil region of the magnet (Q4) immediately downstream of the internal dump. The question being addressed is whether Q4 is expected to quench during routine extraction. Similar calculations were described in a previous note,¹ but since that time the conceptual design of the abort system has undergone considerable revision, and some progress has been made on an engineering design of the dump itself. The conceptual design is described elsewhere.²

II. Description of CASIM Calculation

(A) Geometry

The geometry of the calculation is largely based on a preliminary engineering design by Erwin Rodger. A sketch of the beginning of the dump region is shown in Fig. 1. A slot is shown in this figure through which the aborted beam is kicked. The first material encountered by the aborted beam is a 50 cm. long rectangular block of material known as Carbon-Carbon (C-C). This material, highly resistant to thermal shock, is described in Ref. [2]. Downstream of this block is a thin steel window, and a short transition region followed by a 2m long section of ordinary graphite. After this point the dump is steel to the end of the dump which is 5.2m from the entrance face of the C-C block.

The aperture of the dump from the beginning of the graphite to the end is an ellipse with a semi-major axis of 23 mm. and a semi-minor axis of 21 mm. The thickness of the (steel) beam pipe in the first set of calculations was 1.25 mm, which is followed by a 1.5 mm region for a heater which is present for baking the beam pipe. Analysis of the results of these calculation showed that a major component of the energy deposition in the Q4 coil was due to electromagnetic punch through (mostly photons) which could be reduced by a thicker beam pipe, so another set of calculations was performed with a 3 mm. thick beam pipe. Thus, two "geometries" were considered, differing only in the thickness of the beam pipe in most of the dump region. The 1.5 mm thick heater region, which is mostly insulation, was taken to be carbon with $\rho = 0.5 \text{ g/cc}$.

At the exit of the dump proper, the beam pipe is flared to a vacuum valve flange. Shortly after this flange, the warm to cold transition occurs which was simulated in reasonable detail. The distance from the end of the dump to the vacuum valve flange is 1.4m and the cold mass of the magnet begins 80 cm. after this flange. The reason for simulating this region in detail is that material close to the beam pipe axis is a medium for photon conversion.

The radial approximation of Q4 is given in Table 1 below. The coil region, which extends radially between 4.0 and 5.0 cm, is approximated by reduced density ($\rho = 6.0$ g/cc) copper. The total length of Q4 is taken to be 250 cm. The magnetic field, which is taken as the ideal quadrupole field from $R = 0$ to $R = 4$ cm. and ignored in material regions, is described in the first 70 cm of the magnet by $K(m^{-2}) = .0084$ and in the remainder of the magnet by $K = .0909$. These values are meant to reflect the fact that the first 70 cm. of the Q4 assembly is a trim coil. The small spacing between the actual trim coil and the main coil is ignored.

Table 1 Approximation of Q4 Region

Radial Region (cm)	Material
$R < 3.46$	Vacuum
$3.46 \leq R < 3.66$	Fe: $\rho = 7.6$ g/cc [Beam Pipe]
$3.66 \leq R < 4.00$	C: $\rho = 0.5$ g/cc [Filler - He channel]
$4.00 \leq R < 5.00$	Cu: $\rho = 6.0$ g/cc [Coil]
$5.00 \leq R < 5.97$	C: $\rho = 1.0$ g/cc [Spacer]
$5.97 \leq R < 13.3$	Fe: $\rho = 7.6$ g/cc [Yoke]

The incident beam was taken to be 250 GeV/c protons. This was shown previously¹ to be the worst case as expected. A separate computer program simulated the displacement on the dump face of 53 bunches.³ Each primary in CASIM was sampled randomly from these bunches. A lateral spread within a bunch in both transverse coordinates was simulated,⁴ but the internal divergence was ignored. Unlike the calculations reported in Ref. [1], the calculations here are completely unbiased.

(B) Energy Binning

To explore the spatial dependence of energy deposition within the Q4 coil, the coil region was divided into 20 segments in the Z (beam) direction and 4 segments in the R (radial) direction. The fact that the beam is aborted to one side means that a manifest left-right asymmetry exists. To explore this, a nominal segmentation of the azimuth into 7 regions as shown in Fig. 2 was made. As shown, the up-down symmetry of the geometry has been incorporated into the binning. The positive X-axis in the coordinate system used, or the $\phi = 0^\circ$ side in Fig. 2, is to the *ring-outward* side and the beam is incident on the dump at negative X, i.e., at $\phi = 180^\circ$ in Fig. 3. A preliminary set of CASIM runs showed that the midplane bin on the +X side (bin #1 in Fig. 2) was of primary interest, at least in the "hot spots" of the coil, so that this angular interval was further divided by 2 and by 4 to be able to search for more localized enhancements on the midplane.

III. Results

Before showing the CASIM results for energy density in the Q4 coil some reference is required. We have historically assumed that the quench threshold is 2 mJ/g.⁵ This value was obtained at FNAL with magnets operating at 90% of short sample. Since the RHIC quads operate at 60% of short sample, this assumption is conservative. The 2 mJ/g assumption gives a quench threshold for the design intensity³ of 57×10^{11} protons of 1.315×10^5 GeV/cc-p in the coil material. The quench threshold of the trim coil region is not clear, but there is no reason to believe the quench threshold is any lower than the 2 mJ/g assumption, and several reasons (a nominal operating point of 20% of short sample, lower local magnetic field, and perhaps greater stability due to more He being present in the trim windings) to believe this number is conservative. Also, the recovery time after a trim coil quench might be rapid enough for such an event to be tolerable.

In the figures below the energy deposition density as a function of position as described above is plotted with an associated error bar. The error bar is just the rms deviation from four CASIM runs of 3 million primaries per run. This crude measure of the error may underestimate or overestimate the statistical error in a given bin. Systematic errors are briefly discussed in the last section of this note.

As mentioned above, the most prominent feature of the energy density distribution within the coil region is a pronounced azimuthal asymmetry. This is shown in Fig. 3 for the 1.25 mm beam pipe geometry. Plotted here is the energy density averaged over the radius of the coil vs. the azimuthal bin number (see Fig. 2) for the two Z bins corresponding to the beginning of the trim coil region and the beginning of the main coil region. This asymmetry slowly decreases with magnet length, but so does the value of the energy density at any position, so the midplane azimuthal bin is only one given further consideration.

Fig. 4 shows the energy density in this azimuthal bin vs. Z averaged over R for both the 1.25 mm beam pipe and the 3.0 mm beam pipe geometries. Only the error bars on the highest energy density bins are shown. For the 1.25 mm geometry, the "hot spots" for the trim and main coil regions are seen to be the first Z bins in those regions. For the 3.0 mm geometry, the trim region hot spot was taken as the average of the first two bins. The data in these Z bins were further explored for radial dependence and finer-grained azimuthal dependence as described in II(B) above.

Figs. 5 and 6 show the radial and azimuthal dependence respectively of the Z bin hot spots. In viewing these results, it must be kept in mind that the errors shown are very strongly correlated. With this in mind, it is *likely* that some radial enhancements exist and *possible* that some of the results should have finer azimuthal binning than the nominal 30° width. It seems prudent to *make an allowance* for such enhancements. Table 2 below shows enhancement factors applied to the $\Delta\Phi=30^\circ$, $\Delta R=1$ cm hot spot bins of Fig 4, based on the assumption that the highest 3 ΔR bins⁶, and smallest $\Delta\Phi$ bin should be used.

Table 2 Enhancement Factors to the Basic Energy Binning

Geometry	Position	Radial Factor	Azimuthal Factor	Total
1.25 mm pipe	Trim	1.14	1.07	1.22
	Main	1.06	1.08	1.16
3.00 mm pipe	Trim	1.08	1.08	1.17
	Main	1.17	1.0	1.17

With these modest enhancements, the energy density values, converted to mJ/g at design intensity, is shown in Table 3 below.

Table 3 Maximum Energy Densities in mJ/g at Design Intensity

Geometry	Trim Coil	Main Coil
1.25 mm pipe	2.00 ± 0.27	1.01 ± 0.19
3.00 mm pipe	0.78 ± 0.13	0.40 ± 0.11

The errors in Table 3 are simply the estimate of statistical error from Fig. 4; no error on the enhancement factors is included.

IV. Discussion of Results

The thicker beam pipe appears to offer a significant improvement, and should be implemented if possible. The most difficult problem in calculations such as those described here is evaluating the systematic error. The primary sources for such error are believed to be inaccuracy in the physics simulation in CASIM and inadequate representation of the details of the geometry. An attempt has been made to minimize the latter by simulating the current engineering implementation of the dump design. Based on primarily FNAL experience, a factor of 2 to 3 is considered to be reasonable agreement between CASIM predictions and observations in a geometry as complicated as that considered here. The thick beam pipe geometry gives a safety factor somewhat greater than this for the main coil in this worst-case situation.⁷ Although not explicitly discussed in this note, the energy density is very sensitive to the transverse displacement on the C-C block achieved by the kickers,¹ so that meeting the kicker specification is critically important.

References/Footnotes

1. A.J. Stevens, "Preliminary Study of Energy Deposition Downstream of the Internal Dump," AD/RHIC/RD-33, January, 1992.
2. A.J. Stevens, "Conceptual Design of the RHIC Dump Core," AD/RHIC/RD-94, September, 1995.
3. The kicker rise was taken from simulations performed by Chris Pappas. The 53 bunches assume that there are 4 missing bunches out of the design value of 57. In the normalization in section III, a total design intensity of 57×10^{11} is assumed, in part for historical reasons and in part because of the fact that, in practice, as many bunches will exist as can be safely dumped.
4. The actual bunch spread assumed was appropriate for Au ions at 15π emittance which is equivalent to $\sim 35\pi$ for 250 GeV/c protons. This discrepancy with the nominal 20π emittance is not relevant since the bunches are spread much farther apart by the kicker magnet than the internal bunch size.
5. R. Dixon, N.V. Mokhov, and A. Van Ginneken, "Beam Induced Quench Study of Tevatron Dipoles," Fermilab FN-327, 1980.
6. In the case of the main coil region in the 3 mm. geometry, the first two R bins in Fig. 5 were used.
7. The results of Ref [1] indicate that the maximum energy density for Au ions at 100 GeV/u may be less than the 250 GeV/c proton beam considered here by a factor of 2 to 3.

8/7/95

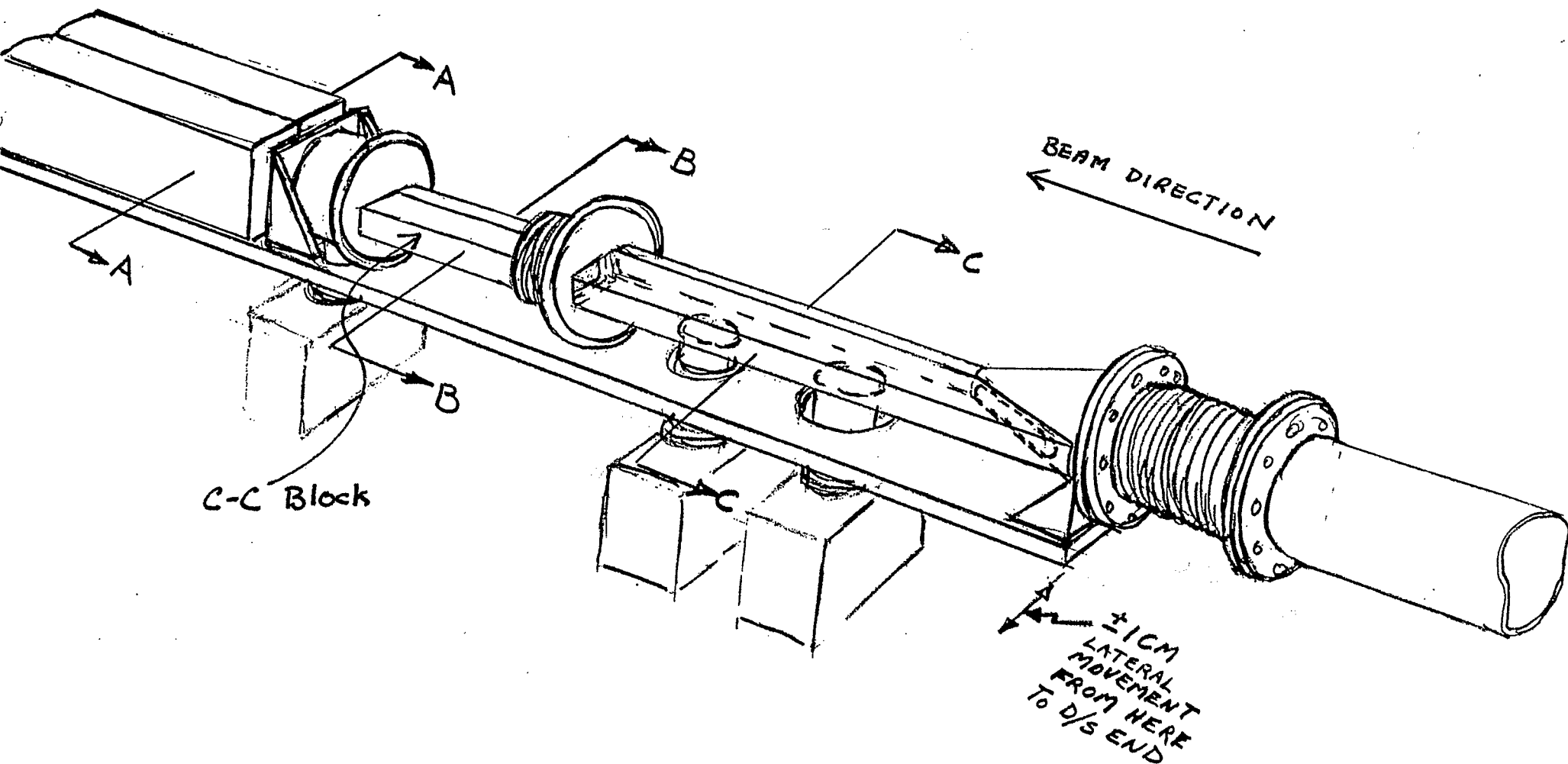


Fig. 1 Preliminary Engineering Sketch of the Dump Region Near its Upstream End. The "dump core" (see Ref [2]) has some lateral adjustment as shown. The "boxes" below the beam pipe indicate vacuum pumps. In the design studied, the most downstream pump shown in this figure was eliminated which reduces the space between the C-C block and the remainder of the dump core to about 3 cm.

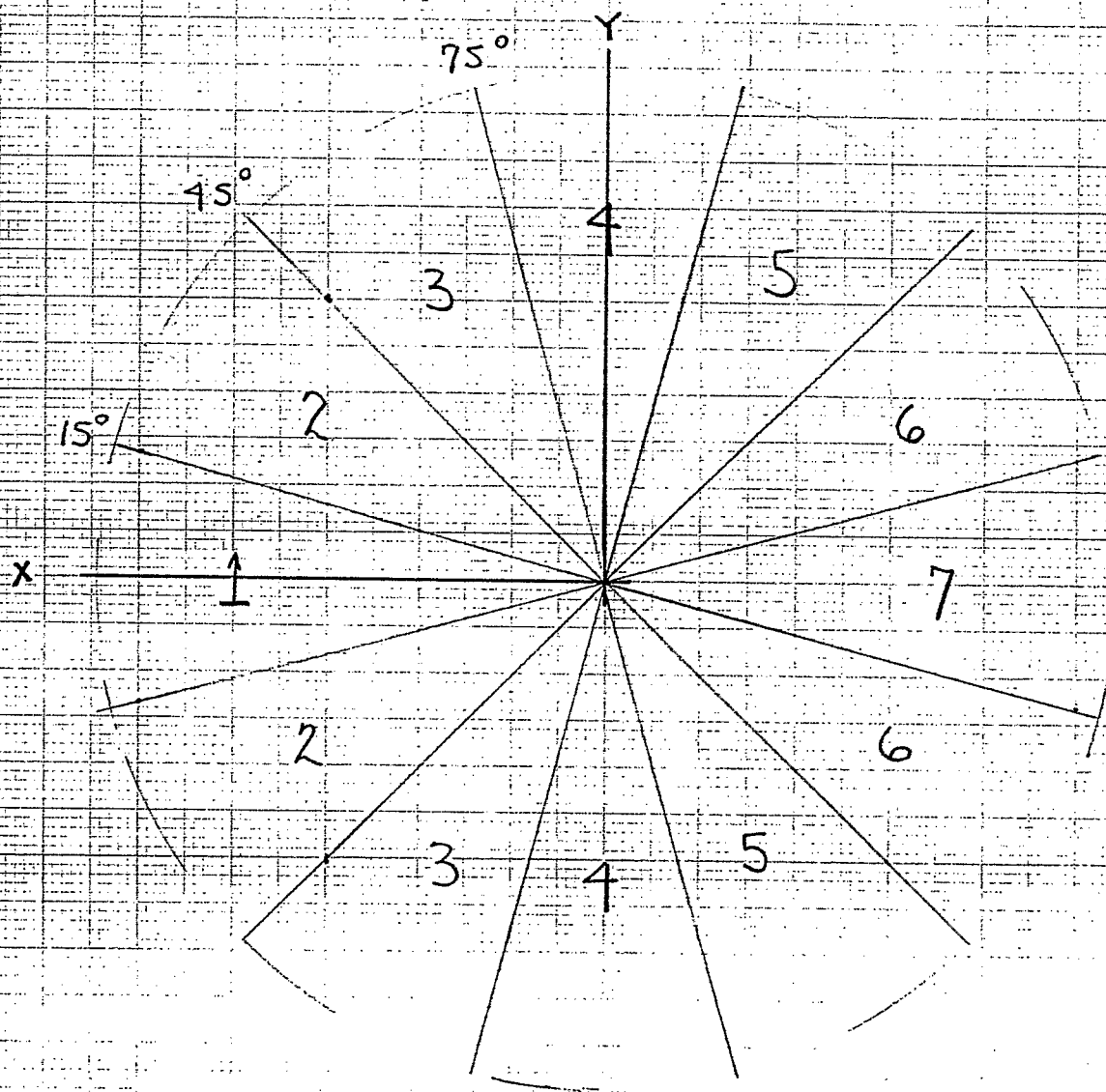


Fig. 2 The 7 Azimuthal Bins Used to Score Energy Deposition.
 The first bin is in the "Ring-outside" direction. The beam is
 incident on the -X (ring-inside) side.

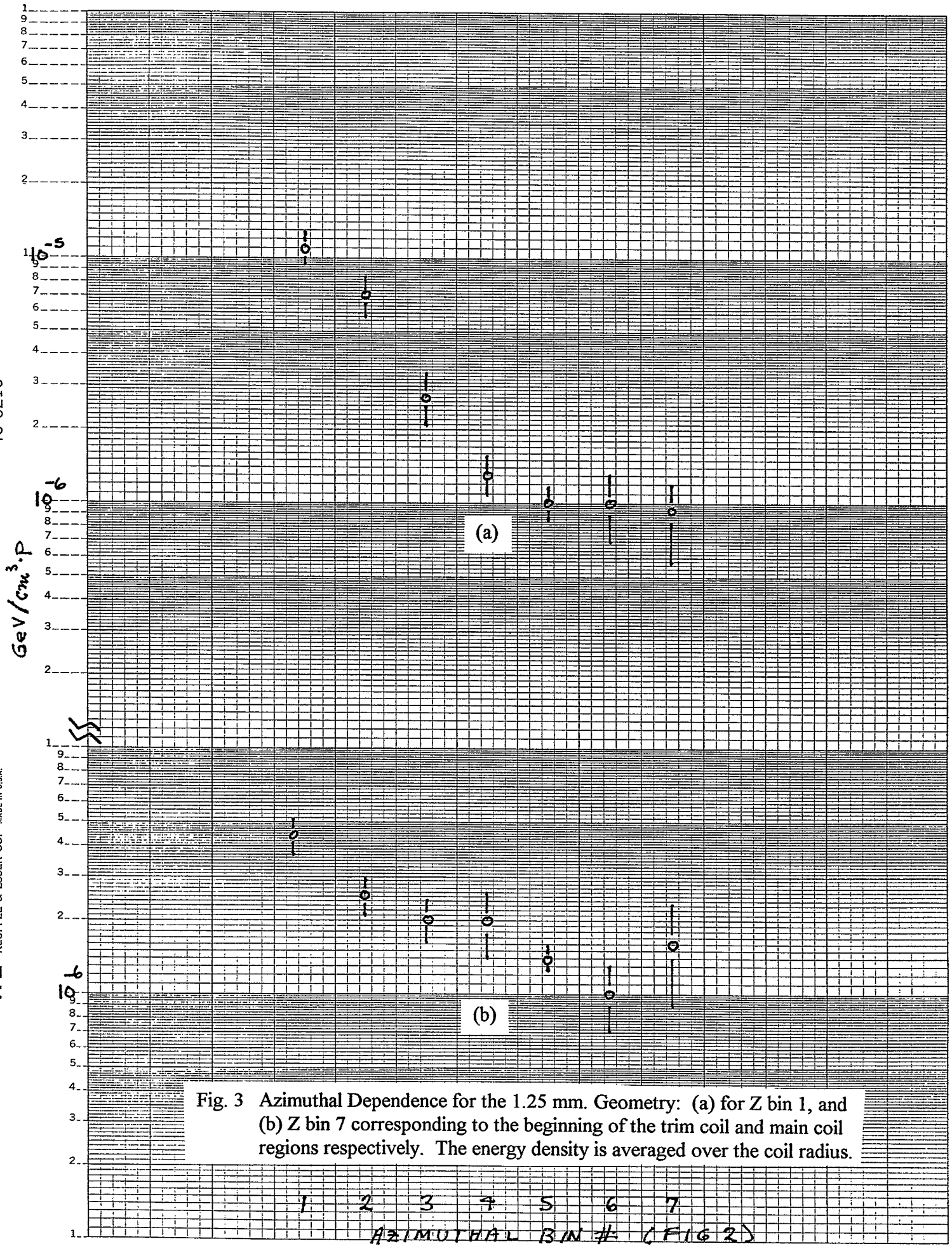


Fig. 3 Azimuthal Dependence for the 1.25 mm. Geometry: (a) for Z bin 1, and (b) Z bin 7 corresponding to the beginning of the trim coil and main coil regions respectively. The energy density is averaged over the coil radius.

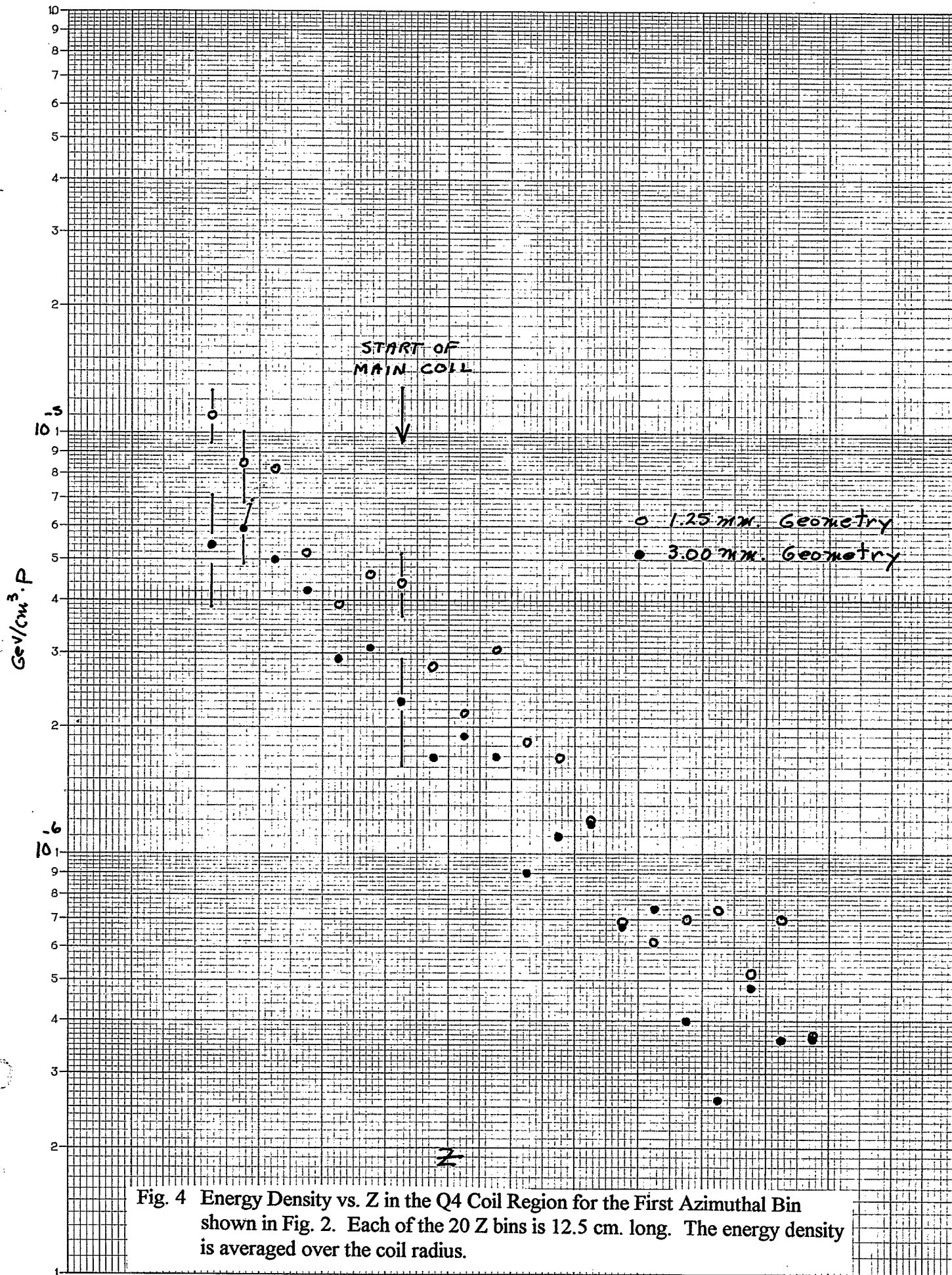


Fig. 4 Energy Density vs. Z in the Q4 Coil Region for the First Azimuthal Bin shown in Fig. 2. Each of the 20 Z bins is 12.5 cm. long. The energy density is averaged over the coil radius.

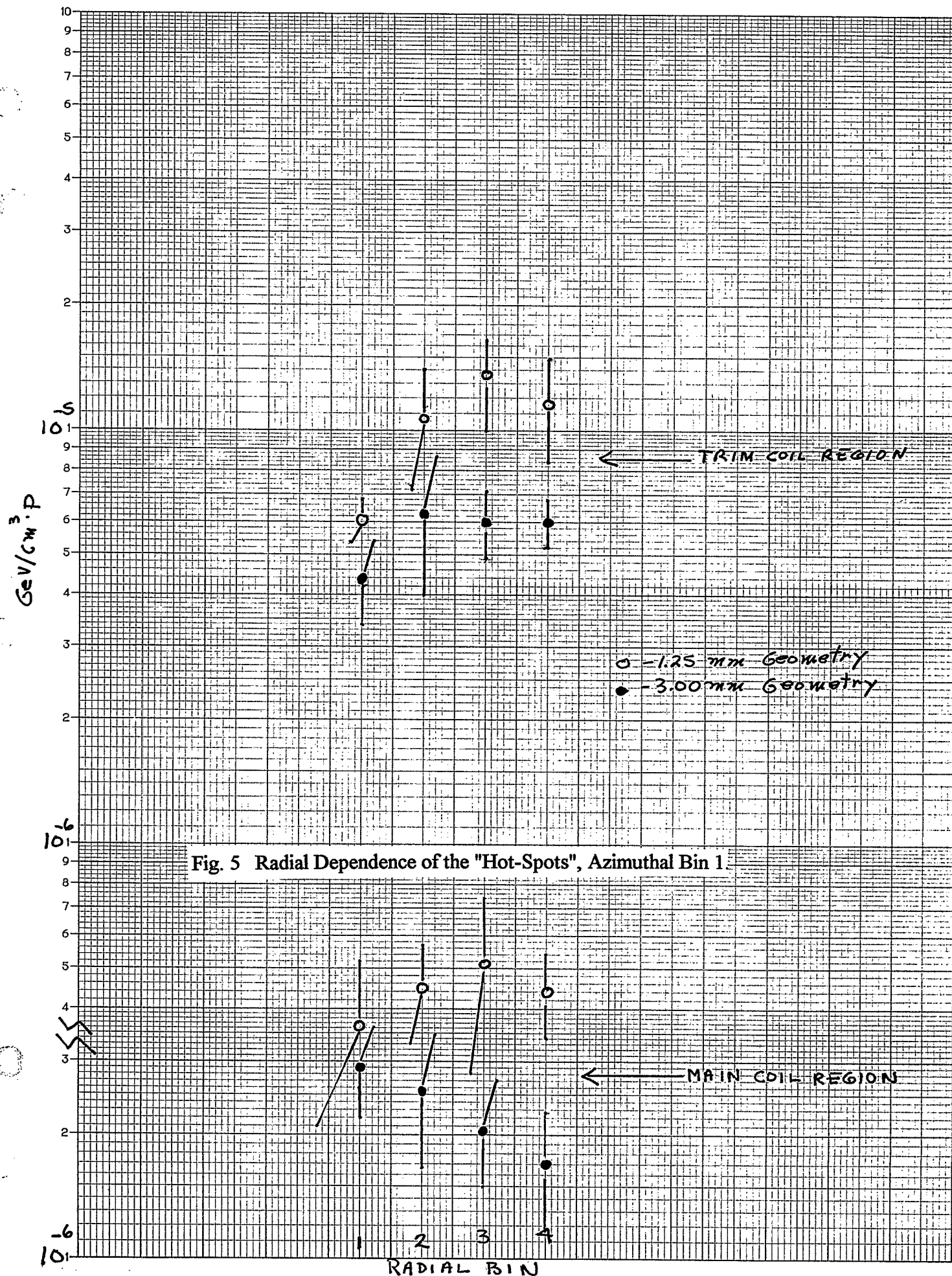


Fig. 5 Radial Dependence of the "Hot-Spots", Azimuthal Bin 1

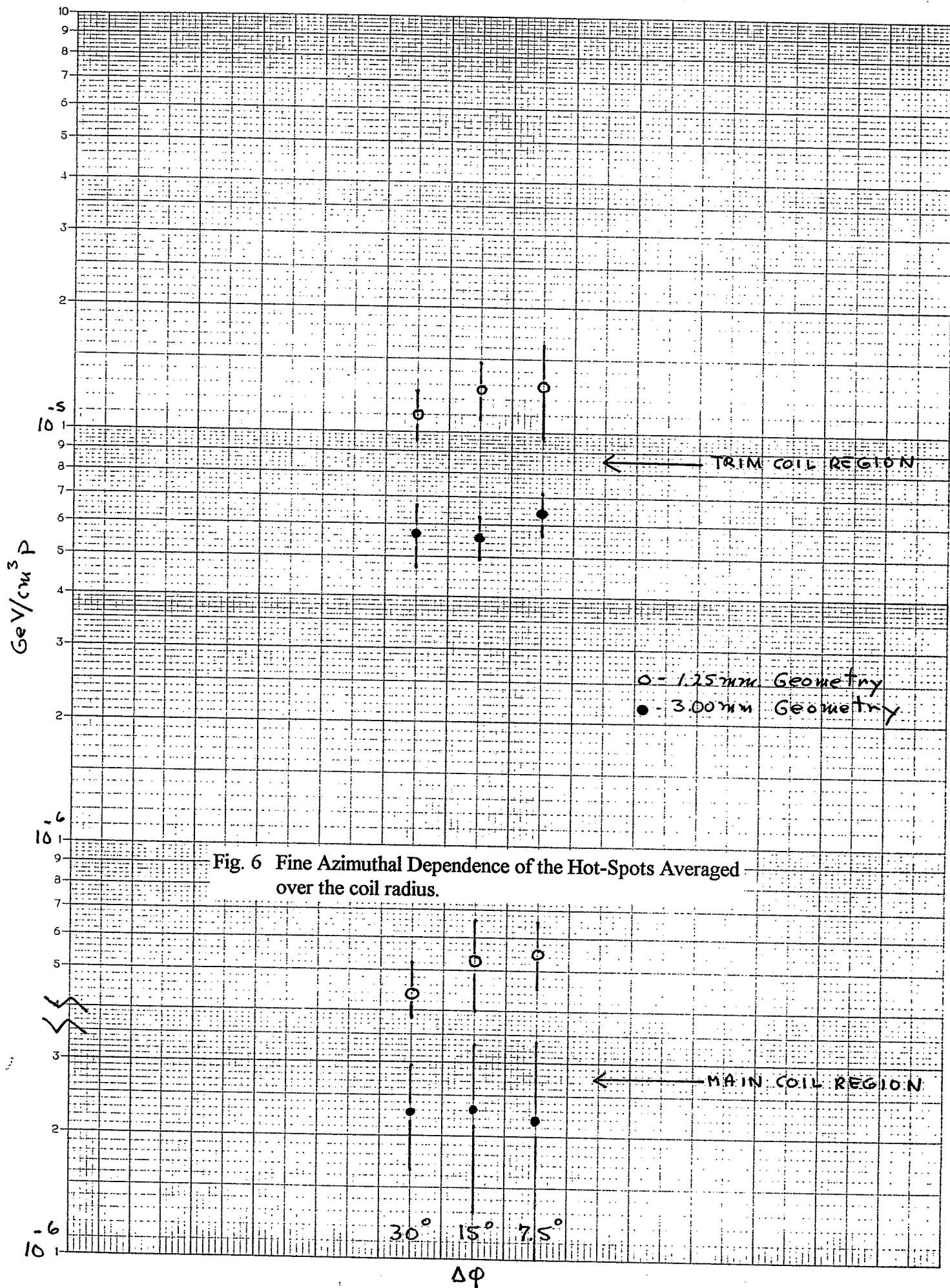


Fig. 6 Fine Azimuthal Dependence of the Hot-Spots Averaged over the coil radius.